FRONTIERS OF PHYSICS

RESEARCH ARTICLE
Volume 18 / Issue 6 / 63305 / 2023

High-sensitive two-dimensional PbI_2 photodetector with ultrashort channel

Kaiyue He[1,2,*], Jijie Zhu[1,*], Zishun Li[2], Zhe Chen[2], Hehe Zhang[1], Chao Liu[1], Xu Zhang[1], Shuo Wang[1], Peiyi Zhao[1], Yu Zhou[1], Shizheng Zhang[1], Yao Yin[1,†], Xiaorui Zheng[2,‡], Wei Huang[1], Lin Wang[1,§]

1 School of Flexible Electronics (Future Technologies) & Institute of Advanced Materials (IAM), Key Laboratory of Flexible Electronics (KLOFE), Jiangsu National Synergetic Innovation Center for Advanced Materials (SICAM), Nanjing Tech University, Nanjing 211816, China

2 Research Center for Industries of the Future (RCIF), School of Engineering, Westlake University, Hangzhou 310030, China

*These authors contributed equally to the work.

Corresponding authors. E-mail: †iamyyin@njtech.edu.cn, ‡zhengxiaorui@westlake.edu.cn, §iamlwang@njtech.edu.cn

Received March 8, 2023; accepted May 12, 2023

ABSTRACT

Photodetectors based on two-dimensional (2D) semiconductors have attracted many research interests owing to their excellent optoelectronic characteristics and application potential for highly integrated applications. However, the unique morphology of 2D materials also restricts the further improvement of the device performance, as the carrier transport is very susceptible to intrinsic and extrinsic environment of the materials. Here, we report the highest responsivity (172 A/W) achieved so far for a PbI_2-based photodetector at room temperature, which is an order of magnitude higher than previously reported. Thermal scanning probe lithography (t-SPL) was used to pattern electrodes to realize the ultrashort channel (~60 nm) in the devices. The shortening of the channel length greatly reduces the probability of the photo-generated carriers being scattered during the transport process, which increases the photocurrent density and thus the responsivity. Our work shows that the combination of emerging processing technologies and 2D materials is an effective route to shrink device size and improve device performance.

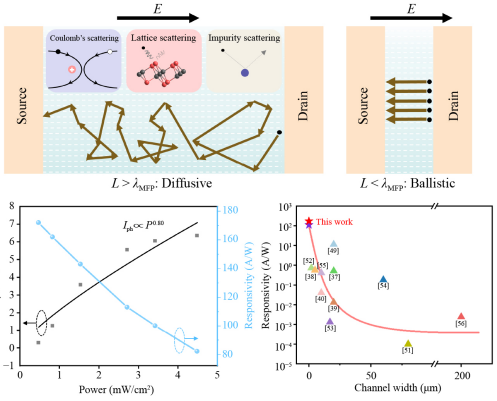

Keywords two-dimensional photodetectors, carrier scattering, ultrashort channel, thermal scanning probe lithography, PbI_2 nanosheets

1 Introduction

Photodetectors have been widely applied in many fields including digital display, biomedical imaging, environment monitoring and so forth [1, 2]. In general, the operation of most photodetectors involves three main processes: light absorption [3, 4], electron–hole pair separation [5, 6], and carrier transport. Although less attention has been paid to carrier transport than the first two in previous studies, it is crucial to the performance of photodetectors. In recent years, two-dimensional (2D) semiconductors have shown great application potential in the photodetectors owing to their unique structures

#Special Topic: Two-dimensional Electronic Materials and Devices (Eds.: Lin Wang & Xiaolong Chen).

Higher Education Press

https://doi.org/10.1007/s11467-023-1323-1

and superior optoelectronic properties [7–10]. Due to the atomic thickness and strong surface/interface effect, the performance of 2D photodetectors is more strongly related to carrier scattering than conventional devices [11]. Carrier scattering, usually caused by lattice vibrations [12–14], ionized impurities [15, 16], and other material disorders [17], is one of the most important factors affecting carrier transport.

Previous studies on 2D electronic devices have shown that when the channel length was shortened to below 100 nm, the carrier scattering would be obviously suppressed and manifested as a significant improvement in the current density. For example, the current density of the MoS_2 field-effect transistors (FETs) was increased by two orders of magnitude by shortening the channel length down to sub-10 nm [18, 19]. Similar phenomenon was also found in WSe_2 transistors. The highest current density ever reported in 2D transition metal dichalcogenides (TMD) transistors to date was realized by fabricating bilayer WSe_2 transistors with sub-100 nm channel-length [20]. Considering 2D semiconductors are immune to short-channel effects, shortening the channel length is also one of the effective means to reduce device size and improve integration [21–23]. Unfortunately, the fabrication of short-channel devices is extremely challenging. At present, the main preparation methods of short-channel devices are either require specific electrode materials [18, 20] or device structures [21, 24–26], or cause unavoidable damage to the fragile 2D materials [27]. Thermal scanning probe lithography (t-SPL) is an emerging direct-write nanolithography method, using thermal energy from a heated nanometer-scaled tip to induce local material modification [28–32]. It enables in situ simultaneous patterning and imaging of 2D materials with sub-10 nm resolution without damaging the materials or contaminating the surface, which is very important for fabricating ultrashort channel devices [33–36]. However, it has not been used in the preparation of 2D photodetectors with ultrashort channel.

In this work, we introduced the t-SPL method to the fabrication of 2D photodetectors for the first time. Multilayered-PbI_2 is a kind of direct-bandgap semiconductors with wide bandgap (~2.5 eV), large absorption coefficient, high resistivity, and large atomic number, which is promising for 2D ultraviolet photodetectors, room-temperature X-ray/γ-ray detectors, and spin-photonics applications [37–44]. However, the performance of PbI_2-based photodetectors has been unsatisfactory due to the suboptimal charge transport. As a good demonstration, the sensitivity of the photodetector based on PbI_2 nanosheet was significantly improved by shortening the channel length to 60 nm. The sharp increase in sensitivity mainly comes from the greatly suppressed carrier scattering brought about by the shortened channel length. In this way, an ultra-high responsivity up to 172 A/W at room temperature was realized, which is one order of magnitude higher than the highest responsivity of previously reported PbI_2-based photodetectors. Our work fully demonstrates that the introduction of advanced processing methods can facilitate the fabrication of ultrashort channel devices and significantly improve their optoelectronic performance. It will also greatly promote the application of 2D semiconductors in high-performance and high-integration optoelectronic devices.

2 Experimental section

Firstly, PbI_2 nanosheets were prepared on PDMS (polydimethylsiloxane) substrate via solution method according to previous report [45, 46] [Fig. 1(a)]. A piece of PbI_2 nanosheet with regular shape, smooth surface, and lateral dimension of approximately 42 μm was selected for the construction of photodetector [Fig. 1(b)].

The patterning of electrodes was processed with the t-SPL method [Fig. 1(c)]. To be specific, the PMGI (polymethylglutarimide) film and heat-sensitive PPA (polyphthalaldehyde) film were spin-coated onto Si/SiO_2 substrate successively to form a dual-polymer stacking as a resist. By precisely controlling the movement of a heated nano-probe (200 °C), etching of the PPA film with ultrahigh resolution can be achieved. The pattern was further etched into the underlying PMGI with TMAH (tetramethylammonium hydroxide) solution. Then a stack of Cr/Au [3 nm/25 nm, provided by ZhongNuo Advanced Material (Beijing) technology Co., Ltd] metals was deposited using electron-beam evaporation. After that, the specimens were soaked in Remover PG for metal lift-off. As can be seen in Fig. 1(d), a metal electrode array with a minimum spacing of 60 nm was realized.

At last, a piece of PbI_2 nanosheet was transferred onto the patterned electrode array followed by a brief annealing in argon at 150 °C for 2 hours to improve the quality of the van der Waals contact between the metal and the semiconductor [Figs. 1(e) and (f)].

3 Results and discussion

With the help of t-SPL method, a 2D PbI_2-based photodetector with a lateral metal–semiconductor–metal configuration and ultrashort channel was fabricated. The schematic diagram of the photodetector is shown in the inset of Fig. 2(a). PbI_2 nanosheets with smooth surfaces were selected for the construction of photodetectors, which can ensure high-quality contact between the nanosheets and electrodes, so that the transport of photogenerated carriers at the interface would not be restricted.

The output characteristic curves of the photodetector were measured in the dark and under laser irradiation

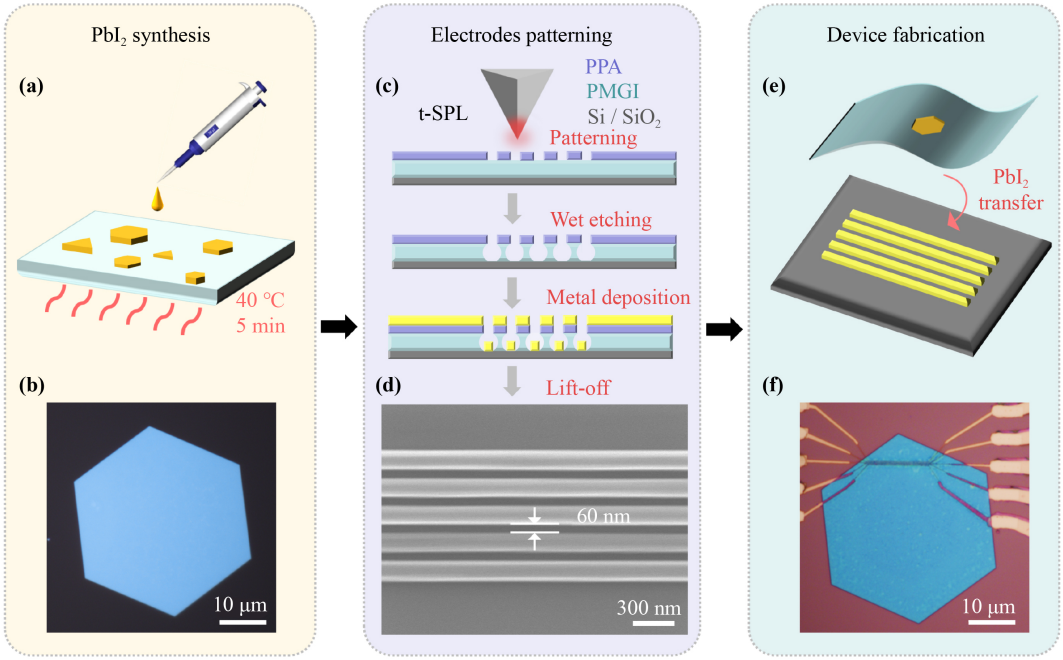

Fig. 1 The fabrication process of PbI_2-based photodetector with ultrashort channel. **(a)** Schematic illustration of synthesizing PbI_2 nanosheets via solution-processed method. **(b)** The optical image of the as-grown PbI_2 nanosheet with regular hexagonal shape and flat surface. **(c)** Schematic illustration of the t-SPL patterning process for the fabrication of metal electrodes with ultrashort spacing. **(d)** SEM image of electrodes with a spacing of 60 nm. **(e)** Schematic illustration of transfer process. **(f)** Optical image of a PbI_2-based photodetector with ultrashort channel.

with different power densities. As shown in Fig. 2(a), source-drain current (I_{ds}) maintains a linear and symmetrical relationship with bias voltage (V_{ds}), proving that a good ohmic contact was formed between the PbI_2 nanosheet and the electrodes. At the same time, with the increase of the incident light power density, I_{ds} corresponding to the same V_{ds} shows a gradual increase trend.

The dependence of the net photocurrent (I_{ph}) on the incident light power (P) can be described by the power law: $I_{ph} \propto P^{\beta}$. The value of the exponent β reflects the utilization rate of the photodetector to the incident light. Figure 2(b) plots the relationship between I_{ph} and P of our photodetector. The fitted exponent β is 0.80, suggesting that there is a photogating effect in our device [38]. The existence of the photogating effect can be further confirmed by the shift of the transfer curve with the change of the gate voltage (V_g) [47] [Fig. S1 of the Electronic Supplementary Materials (ESM)]. The derived responsivity (R) values under different incident power densities were also plotted in Fig. 2(b). The responsivity was derived from $R = \frac{I_{ph}}{PS}$ [38], where S is the effective area of the photodetector. The responsivity as high as 172 A/W was achieved when V_{ds} was 3 V and P was 0.47 mW/cm^2. To the best of our knowledge, it is the highest responsivity ever reported in PbI_2-based photodetectors, which is an order of magnitude higher than the highest responsivity of previously reported devices. Moreover, the responsivity decreases with increasing illumination power, which can be attributed to the higher probability of carrier recombination during transport under high carrier concentration, resulting in a decrease in photocurrent.

It is well-known that the electrical properties of 2D semiconductors can be effectively tuned by an external electric field which is usually generated by applying a vertical bias [48]. Since the devices prepared with t-SPL method usually have a structure in which the electrodes are below the channel, a top gate can be easily added to the fabricated photodetector without any damage to the original device structure [Fig. 2(d) inset]. Here, a photodetector with a top gate was fabricated to study the gate-controlled photodetection performance of photodetectors with ultrashort channel. h-BN was used as the gate dielectric. Considering PbI_2 nanosheet is a p-type semiconductor [4, 49], positive V_g was applied to the photodetector to reduce the concentration of holes in the channel. Comparing the output curves under different V_g [Fig. 2(c)], it can be found that I_{ds} gradually decreases as the positive V_g increases, no matter in the dark or with light illumination (405 nm, 0.36 mW/cm^2).

At the same time, the increase of the positive V_g has a more obvious effect on I_{ds} under light illumination than in the dark, resulting in the responsivity decreases [Fig. 2(d)]. It can be attributed to the above-mentioned photogating effect being suppressed by the applied positive

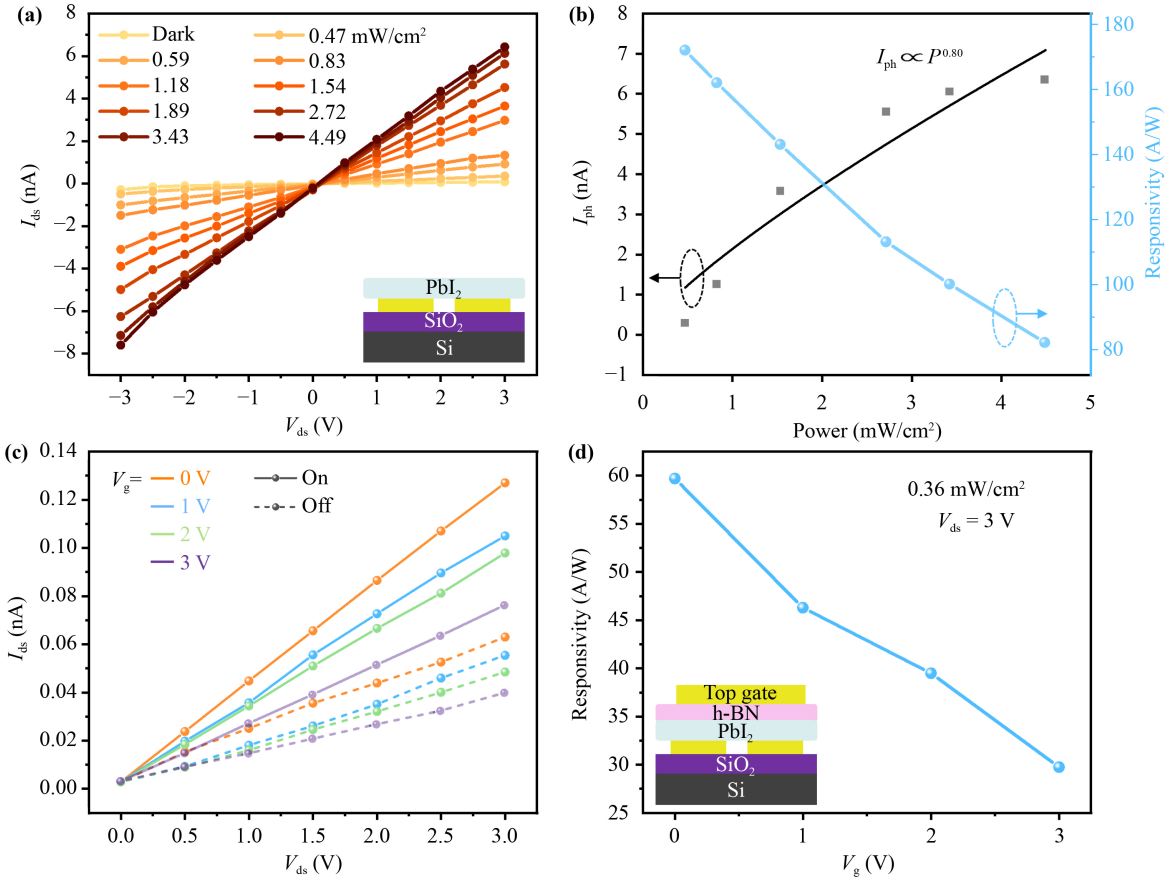

Fig. 2 Photodetection performance of PbI_2-based ultrashort channel photodetector at room temperature. The wavelength of the incident laser is 405 nm. **(a)** I–V characteristics in the dark and under different incident power densities. Inset: A schematic drawing of the configuration of photodetector. **(b)** Photocurrent and responsivity versus incident power density with V_{ds} = 3 V. **(c)** I–V characteristics of photodetector in the dark and under different incident power densities with stepped positive V_g. **(d)** Responsivity as a function of the positive V_g. Inset: Schematic diagram of device structure with a top-gate.

V_g. The photogating effect is a way of modulating the channel conductance with light-induced or electrically-driven gate field. Higher photocurrent can be achieved with the promoted gain, as the lifetime of photo-generated minority carriers is prolonged in low-dimensional channel, where impurities and defects may act as trap centers rather than recombination centers [11, 50]. In our case, when the external positive V_g was applied, these trap centers were quickly filled by the continuously injected electrons from gate. Therefore, the concentration of free photo-generated holes decreased with the increase of the positive V_g, resulting in a drop in the responsivity of the photodetector. In addition, the derived responsivity of photodetectors with top gate were slightly lower than that of non-top-gated devices under the same test conditions. This is because the huge non-transparent metal top gate electrode blocks part of the incident light, so that the actual power density irradiated on the channel is much less than the measured incident power density used in the calculation of responsivity.

In order to investigate the effect of channel length on the responsivity of photodetectors, we summarized and plotted the responsivity as a function of the corresponding channel length of previously reported PbI_2-based photodetectors [37–40, 49, 51–56] (Fig. S2 of the ESM) as shown in Fig. 3(a). It can be observed that the responsivity shows an exponential upward trend with the shortening of channel length, which can be attribute to the significant suppression of carrier scattering in short-channel devices.

As a photoconductive detector, the generation of photocurrent in our device mainly comes from the photo-generated electron–holes pairs [Fig. 3(b)]. The electron–hole pairs are separated by the applied V_{ds}, resulting in the increase of the free carrier concentration in the semiconductor. The efficient transport of free carriers forms the photocurrent. It should be noted that multilayered PbI_2, as a 2D material, has a large specific surface area and strong surface/interface effects, so the carrier transport in photodetectors based on PbI_2 nanosheets is very susceptible to the internal conditions of the material and the external environment, such as lattice vibration,

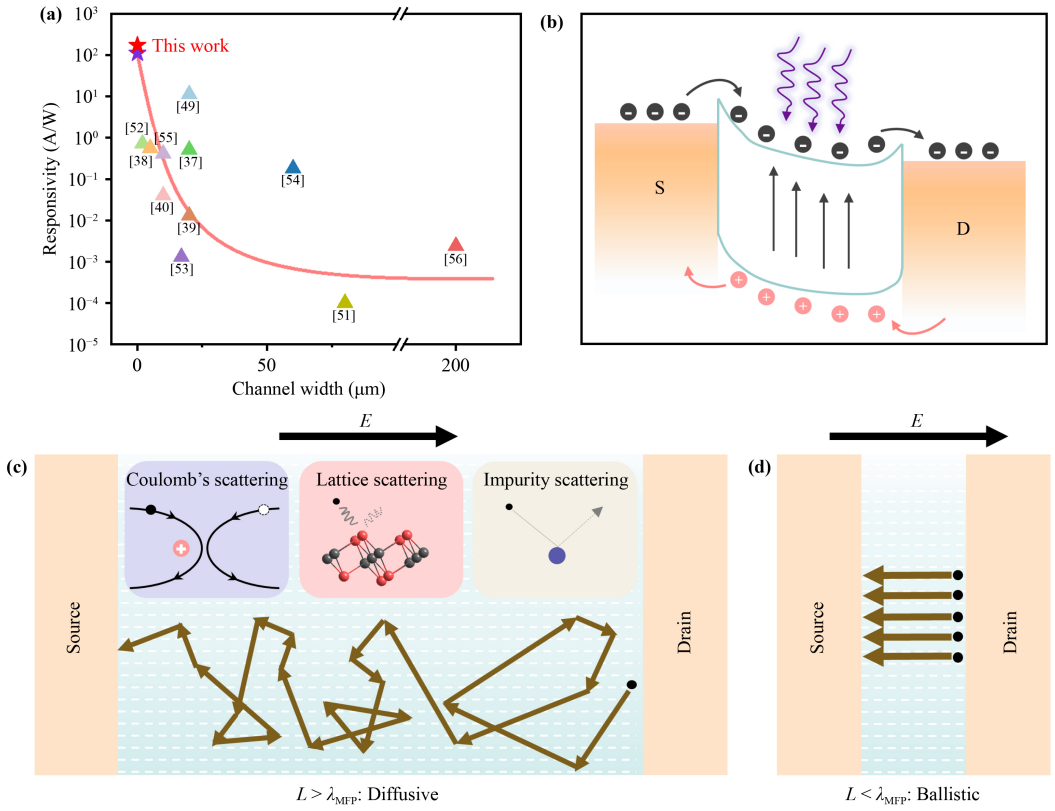

Fig. 3 **(a)** The responsivity of our ultrashort channel photodetector as compared to previous PbI_2-based photodetectors with different channel lengths. **(b)** Schematic image of the photoconductive effect under light illumination in the photodetectors. **(c)** Diffusive transport of carries when the channel length is longer than the λ_{MFP}. The insets show three main scattering mechanisms. **(d)** Ballistic transport when the channel length is shorter than the λ_{MFP}.

atomic defects, strain, adsorbates, surface roughness, and charged impurities [17]. In the long channels whose length is much longer than the mean free path (λ_{MFP}), which is defined as the average distance an electron travels before its momentum is changed by elastic scattering from a static scattering center, the transport of photogenerated carriers would be easily scattered by ionized impurities or remote optical phonons, or collide with electrically neutral impurities to change the transport direction [57] [Fig. 3(c)]. At this time, diffusive transport accounts for a high proportion of charge transport, which seriously reduces the carrier transport efficiency.

When the channel length is shortened to less than the λ_{MFP}, the distance that the photogenerated carriers have to travel before reaching the electrodes was shortened greatly [25]. As a result, the carriers would be hardly scattered by impurities or defects during transport, and the proportion of ballistic transport in carrier transport will be increased significantly [58, 59] [Fig. 3(d)]. As far as photodetectors are concerned, the improvement of carrier transport efficiency will increase not only the density of the current under illumination, but also dark current. Fortunately, since the generation of photocurrent comes from the surge in the number of free carriers, high effective carrier transport would increase the current under illumination much more significantly than the dark current. Therefore, the net photocurrent of short-channel photodetectors will be significantly improved compared with long-channel devices, resulting in a sharp promote in responsivity.

To further study the transport behavior of photogenerated carriers in the channel, temperature-dependent optoelectronic performance characterization was performed. All of the photocurrent was obtained at the V_{ds} of 3 V. The dependence of the photocurrent on the incident power density at different temperatures was demonstrated in Fig. 4(a). It can be observed that the photocurrent always increases gradually with the increase of power density regardless of the varying temperature. The promotion effect of the power increase on the I_{ph} becomes more significant as the temperature decreases, indicating that the transport efficiency of photo-generated carriers is enhanced with the decrease of temperature. The relationships between the derived responsivity and incident power density at different temperatures were shown in Fig. 4(b), which were all consistent with the trend that the responsivity decreases with the increase of power density observed at room temperature.

It is worth mentioning that although shortening the

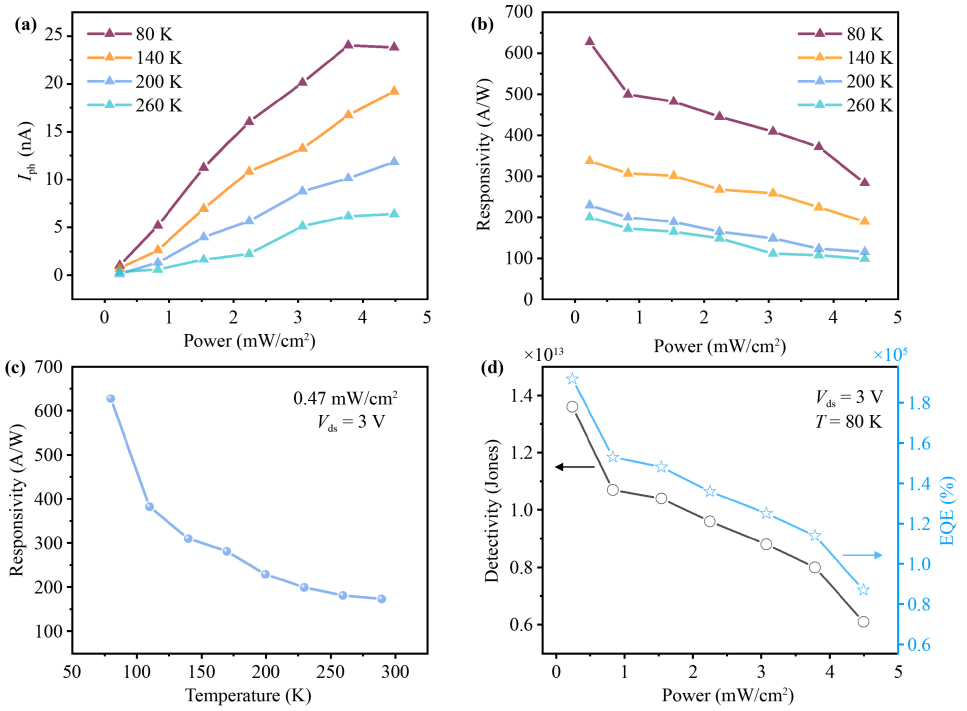

Fig. 4 Temperature-dependent photoelectric characteristics of PbI_2 ultrashort channel photodetector. All data are obtained under 3 V bias. **(a, b)** Photocurrent and responsivity as a function of incident power density at different temperatures. **(c)** Responsivity to incident light with a power density of 0.47 mW/cm^2 at different temperatures. **(d)** Detectivity (black line) and EQE (blue line) as a function of incident power density at 80 K.

channel length can significantly reduce the possibility of carriers being scattered, the ballistic proportion in carrier transport is difficult to reach 100% [60]. The unavoidable interaction between carriers and various intrinsic lattice phonons is the main cause of scattering during transport at room temperature. The probability of phonon scattering of carriers during transport is proportional to $T^{3/2}$, and can be derived from $P_s = \frac{\varepsilon_c^2 k_0 T (m^*)^2}{\pi \rho \hbar^4 u^2} v$, where k_0 is the Boltzmann constant, m^* is the effective mass of the carrier, ρ is the lattice density, u is the velocity of the longitudinal elastic wave, ε_c is the deformation potential constant and v is the velocity of the electron [61]. Hence, the probability of carriers being scattered will further decrease after the temperature drops. We extracted the highest responsivity that the photodetector can achieve at different temperatures, and plotted the relationship between responsivity and temperature [Fig. 4(c)]. As the temperature drops from 290 K to 80 K, the responsivity increases exponentially, reaching the highest responsivity of 627 A/W at 80 K owing to suppressed phonon scattering and more effective carrier transport at low temperature [17, 59].

Detectivity (D^*) and external quantum efficiency (EQE) are two other key parameters to evaluate the

Table 1 Comparison of various figures of merit of different representative PbI_2-based photodetectors.

Morphology	Channel width (μm)	Bias (V)	Incident light (nm)	Responsivity (A·W^{-1})	D^* (Jones)	Ref.
Nanosheet	0.06	3	405	172	4.06 × 10^{12}	This work
Nanosheet	20	5	375	0.51	4.0 × 10^{10}	[37]
Nanosheet	5	5	450	0.56	–	[38]
Nanosheet	10	5	450	0.04	3.31 × 10^{10}	[40]
Nanosheet	80	1.9	450	0.0001	–	[51]
Nanosheet	2	5	470	0.72	1.04 × 10^{10}	[52]
Nanosheet	17	10	405	0.0013	–	[53]
Nanosheet	10	5	405	0.41	3.1 × 10^{11}	[55]
Nanobelt	20	5	445	0.013	–	[39]
Single crystal	20	15	440	11.3	–	[49]
Single crystal	60	10	450	0.18	3.23 × 10^{11}	[54]

photo-sensitivity of a photodetector, and can be given by equations: $D^*=\frac{RS^{1/2}}{(2eI_{dark})1/2}$ and $\mathrm{EQE}=\frac{Rhc}{e\lambda}$ [25] respectively, where I_{dark} is the dark current, e is the electron charge, h is the Plank constant, c is the velocity of light, and λ is the wavelength of incident laser (λ = 405 nm). Figure 4(d) showed the dependence of D^* and EQE on illumination power density with V_{ds} fixed at 3 V. As can be seen, both of D^* and EQE increase with decreasing of power density. At a power density of 0.47 mW/cm^2, D^* and EQE are 1.36 × 10^{13} Jones and 1.92 × 10^5 % respectively, indicating the excellent performance of our PbI_2-based photodetector with ultrashort channel (Table 1).

4 Conclusion

In a word, the shortening of channel length plays an important role in improving the performance of 2D photodetectors. Based on the electrode array with a spacing as short as 60 nm, PbI_2-based photodetector with ultrashort channel was fabricated. It was found that the photodetector exhibits an ultrahigh responsivity of 172 A/W at room temperature and 627 A/W at 80 K, which is an order of magnitude higher than the highest responsivity of the ever-reported PbI_2-based photodetectors. The improvement of responsivity is mainly due to the ultrashort channel length. The shortening of the channel length significantly reduces the probability of scattering during carrier transport, resulting in improved carrier transfer. Our work heralds new possibilities created by the combination of novel processing techniques and 2D semiconductors, which could guide the development of highly integrated optoelectronic devices in the future.

Declarations The authors declare that they have no competing interests and there are no conflicts.

Electronic supplementary materials The online version contains supplementary material available at https://doi.org/10.1007/s11467-023-1323-1 and https://journal.hep.com.cn/fop/EN/10.1007/s11467-023-1323-1.

Acknowledgements The work was financially supported by the National Key R&D Program of China (Grant Nos. 2020YFA0308900 and 2022YFB3602801) and the National Natural Science Foundation References of China (Grant No. 92064010).

References

1. G. Konstantatos, Current status and technological prospect of photodetectors based on two-dimensional materials, *Nat. Commun.* 9(1), 5266 (2018)
2. W. Wu, X. Wang, X. Han, Z. Yang, G. Gao, Y. Zhang, J. Hu, Y. Tan, A. Pan, and C. Pan, Flexible photodetector arrays based on patterned $CH_3NH_3PbI_{3-x}Cl_x$ perovskite film for real-time photosensing and imaging, *Adv. Mater.* 31(3), 1805913 (2019)
3. H. Lin, B. C. P. Sturmberg, K. T. Lin, Y. Yang, X. Zheng, T. K. Chong, C. M. de Sterke, and B. Jia, A 90-nm-thick graphene metamaterial for strong and extremely broadband absorption of unpolarized light, *Nat. Photonics* 13(4), 270 (2019)
4. M. Shkir, I. S. Yahia, V. Ganesh, Y. Bitla, I. M. Ashraf, A. Kaushik, and S. AlFaify, A facile synthesis of Au-nanoparticles decorated PbI_2 single crystalline nanosheets for optoelectronic device applications, *Sci. Rep.* 8(1), 13806 (2018)
5. Q. Fu, X. Wang, F. Liu, Y. Dong, Z. Liu, S. Zheng, A. Chaturvedi, J. Zhou, P. Hu, Z. Zhu, F. Bo, Y. Long, and Z. Liu, Ultrathin Ruddlesden–Popper perovskite heterojunction for sensitive photodetection, *Small* 15(39), 1902890 (2019)
6. X. Zhang, Z. Li, T. Yan, L. Su, and X. Fang, Phase-modulated multidimensional perovskites for high-sensitivity self-powered UV photodetectors, *Small* 19(9), 2206310 (2023)
7. O. Lopez-Sanchez, D. Lembke, M. Kayci, A. Radenovic, and A. Kis, Ultrasensitive photodetectors based on monolayer MoS_2, *Nat. Nanotechnol.* 8(7), 497 (2013)
8. W. Guo, Z. Dong, Y. Xu, C. Liu, D. Wei, L. Zhang, X. Shi, C. Guo, H. Xu, G. Chen, L. Wang, K. Zhang, X. Chen, and W. Lu, Sensitive terahertz detection and imaging driven by the photothermoelectric effect in ultrashort-channel black phosphorus devices, *Adv. Sci. (Weinh.)* 7(5), 1902699 (2020)
9. Y. Cai, J. Yang, F. Wang, S. Li, Y. Wang, X. Zhan, F. Wang, R. Cheng, Z. Wang, and J. He, Ultrasensitive solar-blind ultraviolet detection and optoelectronic neuromorphic computing using α-In_2Se_3 phototransistors, *Front. Phys.* 18(3), 33308 (2023)
10. S. Li, Y. Zhang, W. Yang, H. Liu, and X. Fang, 2D perovskite $Sr_2Nb_3O_{10}$ for high-performance UV photodetectors, *Adv. Mater.* 32(7), 1905443 (2020)
11. D. Kufer and G. Konstantatos, Highly sensitive, encapsulated MoS_2 photodetector with gate controllable gain and speed, *Nano Lett.* 15(11), 7307 (2015)
12. S. G. Menabde, H. Cho, and N. Park, Interface defect-assisted phonon scattering of hot carriers in graphene, *Phys. Rev. B* 96(7), 075426 (2017)
13. J. Gao, A. M. Rao, H. Li, J. Zhang, and O. Chen, Carrier transport dynamics in high speed black phosphorus photodetectors, *ACS Photonics* 5(4), 1412 (2018)
14. Y. Tian, Y. Cheng, J. Huang, S. Zhang, H. Dong, G. Wang, J. Chen, J. Wu, Z. Yin, and X. Zhang, Epitaxial growth of large area ZrS_2 2D semiconductor films on sapphire for optoelectronics, *Nano Res.* 15(7), 6628 (2022)
15. S. J. Kim, B. Park, S. H. Noh, H. S. Yoon, J. Oh, S. Yoo, K. Kang, B. Han, and S. C. Jun, Carrier scattering in quasi-free standing graphene on hexagonal boron nitride, *Nanoscale* 9(41), 15934 (2017)
16. J. H. Chen, C. Jang, S. Adam, M. S. Fuhrer, E. D. Williams, and M. Ishigami, Charged-impurity scattering in graphene, *Nat. Phys.* 4(5), 377 (2008)
17. D. Rhodes, S. H. Chae, R. Ribeiro-Palau, and J. Hone, Disorder in van der Waals heterostructures of 2D mate-

rials, *Nat. Mater.* 18(6), 541 (2019)
18. L. Xie, M. Liao, S. Wang, H. Yu, L. Du, J. Tang, J. Zhao, J. Zhang, P. Chen, X. Lu, G. Wang, G. Xie, R. Yang, D. Shi, and G. Zhang, Graphene-contacted ultrashort channel monolayer MoS_2 transistors, *Adv. Mater.* 29(37), 1702522 (2017)
19. J. Tian, Q. Wang, X. Huang, J. Tang, Y. Chu, S. Wang, C. Shen, Y. Zhao, N. Li, J. Liu, Y. Ji, B. Huang, Y. Peng, R. Yang, W. Yang, K. Watanabe, T. Taniguchi, X. Bai, D. Shi, L. Du, and G. Zhang, Scaling of MoS_2 transistors and inverters to sub-10 nm channel length with high performance, *Nano Lett.* 23(7), 2764 (2023)
20. R. Wu, Q. Tao, J. Li, W. Li, Y. Chen, Z. Lu, Z. Shu, B. Zhao, H. Ma, Z. Zhang, X. Yang, B. Li, H. Duan, L. Liao, Y. Liu, X. Duan, and X. Duan, Bilayer tungsten diselenide transistors with on-state currents exceeding 1.5 milliamperes per micrometre, *Nat. Electron.* 5(8), 497 (2022)
21. F. Wu, J. Ren, Y. Yang, Z. Yan, H. Tian, G. Gou, X. Wang, Z. Zhang, X. Yang, X. Wu, and T. L. Ren, A 10 nm short channel MoS_2 transistor without the resolution requirement of photolithography, *Adv. Electron. Mater.* 7(12), 2100543 (2021)
22. Y. Wang, J. C. Kim, R. J. Wu, J. Martinez, X. Song, J. Yang, F. Zhao, A. Mkhoyan, H. Y. Jeong, and M. Chhowalla, Van der Waals contacts between three-dimensional metals and two-dimensional semiconductors, *Nature* 568(7750), 70 (2019)
23. Y. Liu, X. Duan, Y. Huang, and X. Duan, Two-dimensional transistors beyond graphene and TMDCs, *Chem. Soc. Rev.* 47(16), 6388 (2018)
24. G. Zhang, J. Zhong, Q. Chen, Y. Yan, H. Chen, and T. Guo, High-performance organic phototransistors with vertical structure design, *IEEE Trans. Electron Dev.* 66(4), 1815 (2019)
25. G. Han, S. Cao, Q. Yang, W. Yang, T. Guo, and H. Chen, High-performance all-solution-processed flexible photodetector arrays based on ultrashort channel amorphous oxide semiconductor transistors, *ACS Appl. Mater. Interfaces* 10(47), 40631 (2018)
26. H. Zhang, Y. Zhang, X. Song, Y. Yu, M. Cao, Y. Che, H. Dai, J. Yang, X. Ding, G. Zhang, and J. Yao, Short channel quantum dot vertical and lateral phototransistors, *Adv. Opt. Mater.* 5(2), 1600434 (2017)
27. R. Zan, Q. M. Ramasse, R. Jalil, T. Georgiou, U. Bangert, and K. S. Novoselov, Control of radiation damage in MoS_2 by graphene encapsulation, *ACS Nano* 7(11), 10167 (2013)
28. X. Zheng, A. Calo, T. Cao, X. Liu, Z. Huang, P. M. Das, M. Drndic, E. Albisetti, F. Lavini, T. D. Li, V. Narang, W. P. King, J. W. Harrold, M. Vittadello, C. Aruta, D. Shahrjerdi, and E. Riedo, Spatial defects nanoengineering for bipolar conductivity in MoS_2, *Nat. Commun.* 11(1), 3463 (2020)
29. E. Albisetti, D. Petti, M. Pancaldi, M. Madami, S. Tacchi, J. Curtis, W. P. King, A. Papp, G. Csaba, W. Porod, P. Vavassori, E. Riedo, and R. Bertacco, Nanopatterning reconfigurable magnetic landscapes via thermally assisted scanning probe lithography, *Nat. Nanotechnol.* 11(6), 545 (2016)
30. E. Albisetti, K. M. Carroll, X. Lu, J. E. Curtis, D. Petti, R. Bertacco, and E. Riedo, Thermochemical scanning probe lithography of protein gradients at the nanoscale, *Nanotechnology* 27(31), 315302 (2016)
31. K. M. Carroll, A. J. Giordano, D. Wang, V. K. Kodali, J. Scrimgeour, W. P. King, S. R. Marder, E. Riedo, and J. E. Curtis, Fabricating nanoscale chemical gradients with thermochemical nanolithography, *Langmuir* 29(27), 8675 (2013)
32. E. Albisetti, D. Petti, G. Sala, R. Silvani, S. Tacchi, S. Finizio, S. Wintz, A. Calò, X. Zheng, J. Raabe, E. Riedo, and R. Bertacco, Nanoscale spin-wave circuits based on engineered reconfigurable spin-textures, *Commun. Phys.* 1(1), 56 (2018)
33. K. M. Carroll, X. Lu, S. Kim, Y. Gao, H. J. Kim, S. Somnath, L. Polloni, R. Sordan, W. P. King, J. E. Curtis, and E. Riedo, Parallelization of thermochemical nanolithography, *Nanoscale* 6(3), 1299 (2014)
34. Y. K. Ryu Cho, C. D. Rawlings, H. Wolf, M. Spieser, S. Bisig, S. Reidt, M. Sousa, S. R. Khanal, T. D. B. Jacobs, and A. W. Knoll, Sub-10 nanometer feature size in silicon using thermal scanning probe lithography, *ACS Nano* 11(12), 11890 (2017)
35. R. Garcia, A. W. Knoll, and E. Riedo, Advanced scanning probe lithography, *Nat. Nanotechnol.* 9(8), 577 (2014)
36. X. Liu, Z. Huang, X. Zheng, D. Shahrjerdi, and E. Riedo, Nanofabrication of graphene field-effect transistors by thermal scanning probe lithography, *APL Mater.* 9(1), 011107 (2021)
37. H. Xiao, T. Liang, and M. Xu, Growth of ultraflat PbI_2 nanoflakes by solvent evaporation suppression for high-performance UV photodetectors, *Small* 15(33), 1901767 (2019)
38. Z. Qi, T. Yang, D. Li, H. Li, X. Wang, X. Zhang, F. Li, W. Zheng, P. Fan, X. Zhuang, and A. Pan, High-responsivity two-dimensional p-PbI_2/n-WS_2 vertical heterostructure photodetectors enhanced by photogating effect, *Mater. Horiz.* 6(7), 1474 (2019)
39. M. Han, J. Sun, L. Bian, Z. Wang, L. Zhang, Y. Yin, Z. Gao, F. Li, Q. Xin, L. He, N. Han, A. Song, and Z. X. Yang, Two-step vapor deposition of self-catalyzed large-size PbI_2 nanobelts for high-performance photodetectors, *J. Mater. Chem. C* 6(21), 5746 (2018)
40. R. Wang, S. Li, P. Wang, J. Xiu, G. Wei, M. Sun, Z. Li, Y. Liu, and M. Zhong, PbI_2 nanosheets for photodetectors via the facile cooling thermal supersaturation solution method, *J. Phys. Chem. C* 123(14), 9609 (2019)
41. J. Zhang, Y. Huang, Z. Tan, T. Li, Y. Zhang, K. Jia, L. Lin, L. Sun, X. Chen, Z. Li, C. Tan, J. Zhang, L. Zheng, Y. Wu, B. Deng, Z. Chen, Z. Liu, and H. Peng, Flexible photodetectors: Low-temperature heteroepitaxy of 2D PbI_2/graphene for large-area flexible photodetectors, *Adv. Mater.* 30(36), 1803194 (2018)
42. D. Zhang, Y. Liu, M. He, A. Zhang, S. Chen, Q. Tong, L. Huang, Z. Zhou, W. Zheng, M. Chen, K. Braun, A. J. Meixner, X. Wang, and A. Pan, Room temperature near unity spin polarization in 2D van der Waals heterostructures, *Nat. Commun.* 11(1), 4442 (2020)
43. H. Sun, B. Zhao, D. Yang, P. Wangyang, X. Gao, and X. Zhu, Flexible X-ray detector based on sliced lead iodide crystal, *Phys. Status Solidi Rapid Res. Lett.* 11(2), 1600397 (2017)

44. S. Roth and W. R. Willig, Lead iodide nuclear particle detectors, *Appl. Phys. Lett.* 18(8), 328 (1971)
45. Y. Sun, Z. Zhou, Z. Huang, J. Wu, L. Zhou, Y. Cheng, J. Liu, C. Zhu, M. Yu, P. Yu, W. Zhu, Y. Liu, J. Zhou, B. Liu, H. Xie, Y. Cao, H. Li, X. Wang, K. Liu, X. Wang, J. Wang, L. Wang, and W. Huang, Band structure engineering of interfacial semiconductors based on atomically thin lead iodide crystals, *Adv. Mater.* 31(17), 1806562 (2019)
46. D. Zhou, P. Zhao, J. Zhang, X. Jiang, S. Qin, X. Zhang, R. Jiang, Y. Deng, H. Jiang, G. Zhan, Y. Luo, H. Ma, and L. Wang, Lithographic multicolor patterning on hybrid perovskites for nano-optoelectronic applications, *Small* 18(48), 2205227 (2022)
47. M. Long, P. Wang, H. Fang, and W. Hu, Progress, challenges, and opportunities for 2D material based photodetectors, *Adv. Funct. Mater.* 29(19), 1803807 (2019)
48. F. Xue, Z. Wang, Y. Hou, L. Gu, and R. Wu, Control of magnetic properties of $MnBi_2Te_4$ using a van der Waals ferroelectric III_2–VI_3 film and biaxial strain, *Phys. Rev. B* 101(18), 184426 (2020)
49. J. Zhang, T. Song, Z. Zhang, K. Ding, F. Huang, and B. Sun, Layered ultrathin PbI_2 single crystals for high sensitivity flexible photodetectors, *J. Mater. Chem. C* 3(17), 4402 (2015)
50. M. M. Furchi, D. K. Polyushkin, A. Pospischil, and T. Mueller, Mechanisms of photoconductivity in atomically thin MoS_2, *Nano Lett.* 14(11), 6165 (2014)
51. W. Zheng, Z. Zhang, R. Lin, K. Xu, J. He, and F. Huang, High-crystalline 2D layered PbI_2 with ultrasmooth surface: Liquid-phase synthesis and application of high-speed photon detection, *Adv. Electron. Mater.* 2(11), 1600291 (2016)
52. Y. Wang, L. Gan, J. Chen, R. Yang, and T. Zhai, Achieving highly uniform two-dimensional PbI_2 flakes for photodetectors via space confined physical vapor deposition, *Sci. Bull. (Beijing)* 62(24), 1654 (2017)
53. R. Frisenda, J. O. Island, J. L. Lado, E. Giovanelli, P. Gant, P. Nagler, S. Bange, J. M. Lupton, C. Schuller, A. J. Molina-Mendoza, L. Aballe, M. Foerster, T. Korn, M. Angel Nino, D. P. de Lara, E. M. Perez, J. Fernandez-Rossier, and A. Castellanos-Gomez, Characterization of highly crystalline lead iodide nanosheets prepared by room-temperature solution processing, *Nanotechnology* 28(45), 455703 (2017)
54. Q. Wei, B. Shen, Y. Chen, B. Xu, Y. Xia, J. Yin, and Z. Liu, Large-sized PbI_2 single crystal grown by co-solvent method for visible-light photo-detector application, *Mater. Lett.* 193(15), 101 (2017)
55. C. Lan, R. Dong, Z. Zhou, L. Shu, D. Li, S. Yip, and J. C. Ho, Large-scale synthesis of freestanding layer-structured PbI_2 and $MAPbI_3$ nanosheets for high-performance photodetection, *Adv. Mater.* 29(39), 1702759 (2017)
56. S. Yang, J. Han, J. Zhang, Y. Kong, and H. Liu, In situ growth of PbS/PbI_2 heterojunction and its photoelectric properties, *Nanomaterials (Basel)* 12(4), 681 (2022)
57. P. A. Lemieux, M. Vera, and D. J. Durian, Diffusing-light spectroscopies beyond the diffusion limit: The role of ballistic transport and anisotropic scattering, *Phys. Rev. E* 57(4), 4498 (1998)
58. L. Banszerus, M. Schmitz, S. Engels, M. Goldsche, K. Watanabe, T. Taniguchi, B. Beschoten, and C. Stampfer, Ballistic transport exceeding 28 μm in CVD grown graphene, *Nano Lett.* 16(2), 1387 (2016)
59. P. Luo, C. Liu, J. Lin, X. Duan, W. Zhang, C. Ma, Y. Lv, X. Zou, Y. Liu, F. Schwierz, W. Qin, L. Liao, J. He, and X. Liu, Molybdenum disulfide transistors with enlarged van der Waals gaps at their dielectric interface via oxygen accumulation, *Nat. Electron.* 5(12), 849 (2022)
60. J. Jiang, L. Xu, C. Qiu, and L. M. Peng, Ballistic two-dimensional InSe transistors, *Nature* 616(7957), 470 (2023)
61. J. Bardeen and W. Shockley, Deformation potentials and mobilities in non-polar crystals, *Phys. Rev.* 80(1), 72 (1950)